THE JOURNAL OF PHYSICAL CHEMISTRY B

Article

pubs.acs.org/JPCB

Reaction Mechanism of Zinc-Dependent Cytosine Deaminase from *Escherichia coli*: A Quantum-Chemical Study

Bianca Manta,[†] Frank M. Raushel,[‡] and Fahmi Himo*[,†]

[†]Department of Organic Chemistry, Arrhenius Laboratory, Stockholm University, SE-106 91 Stockholm, Sweden

[‡]Department of Chemistry, Texas A&M University, P.O. Box 30012, College Station, Texas 77842-3012, United States

Supporting Information

ABSTRACT: The reaction mechanism of cytosine deaminase from *Escherichia coli* is studied using density functional theory. This zinc-dependent enzyme catalyzes the deamination of cytosine to form uracil and ammonia. The calculations give a detailed description of the catalytic mechanism and establish the role of important active-site residues. It is shown that Glu217 is essential for the initial deprotonation of the metal-bound water nucleophile and the subsequent protonation of the substrate. It is also demonstrated that His246 is unlikely to function as a proton shuttle in the nucleophile activation step, as previously proposed. The steps that follow are nucleophilic attack by the metal-bound hydroxide, protonation of the leaving group assisted by Asp313, and C−N bond cleavage. The calculated overall barrier is in good agreement with the experimental findings. Finally, the calculations reproduce the experimentally determined inverse solvent deuterium isotope effect, which further corroborates the suggested reaction mechanism.

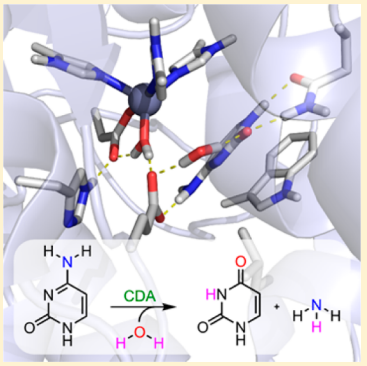

I. INTRODUCTION

Cytosine deaminase (CDA) catalyzes the deamination of cytosine to uracil and ammonia (Scheme 1). CDA from

Scheme 1. Reaction Catalyzed by CDA

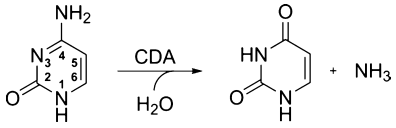

Escherichia coli is a member of the amidohydrolase superfamily (AHS) of enzymes and belongs to cog0402 within the clusters of orthologous groups. Nearly all of the functionally annotated enzymes within cog0402 catalyze the deamination of aromatic bases. Prominent examples include enzymes that deaminate guanine, 8-oxoguanine, *S*-adenosyl homocysteine, thiomethyl adenosine, pterin, and *N*-forminino-L-glutamate.[1] In addition, many other deaminases (adenosine and adenine) are found within cog1816 of the AHS. All of the structurally characterized members of cog0402 fold as a distorted $(\beta/\alpha)_8$-barrrel and contain a mononuclear metal center at the C-terminal end of the β-barrel.[1] All of the deaminases within cog0402 contain three absolutely conserved residues within the active site. These residues include an aspartate that is positioned at the end of β-strand 8, a histidine at the end of β-strand 6, and a glutamate at the end of β-strand 5 of the β-barrel. These three residues and the metal center function in concert with one another to activate the metal-bound water molecule for nucleophilic attack and to facilitate the obligatory protonation of the two reaction products. The focus of this investigation is directed toward a more precise description of the reaction mechanism for the deamination of cytosine by CDA. The molecular details of this study will be directly applicable to the reactions catalyzed by the other deaminases contained within cog0402 and cog1816 because the constellation of residues within the active sites of these enzymes is virtually identical.

High-resolution X-ray structures of CDA have been determined in the presence and absence of tight binding inhibitors that resemble intermediates that are formed during the transformation from substrates to products.[2,3] The most potent of these inhibitors is phosphonocytosine (Scheme 2),

Scheme 2. Tetrahedral Phosphonate Inhibitor of CDA

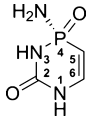

and it binds to CDA with a K_i of 52 nM.[2] This compound mimics the tetrahedral intermediate that is formed directly after the attack of hydroxide at C4 of cytosine. The high-resolution crystal structure of this compound in the active site of CDA provides a detailed view of how the active-site residues are positioned with respect to this inhibitor (Figure 1) and serves as the starting point for the formulation of a detailed mechanism of action. In a previously proposed chemical mechanism, the reaction catalyzed by CDA is initiated by the transfer of a proton from the metal-bound water molecule to

Received: February 4, 2014
Revised: April 7, 2014
Published: May 6, 2014

   dx.doi.org/10.1021/jp501228s | *J. Phys. Chem. B* 2014, 118, 5644−5652

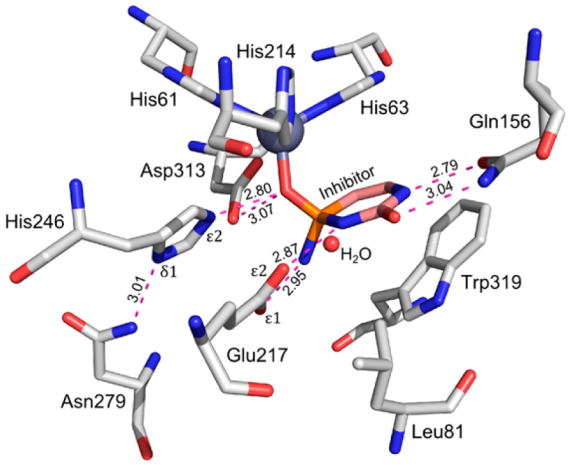

Figure 1. Crystal structure of the active site of CDA from *Escherichia coli* in complex with phosphonocytosine (coordinates taken from PDB entry 3O7U).[2] Distances are given in angstroms.

the side-chain carboxylate of Glu217 with the formation of a metal-bound hydroxide.[2] The tetrahedral intermediate is generated by nucleophilic attack of the metal-bound hydroxide and protonation of N3 by Glu217. Collapse of the tetrahedral intermediate occurs after a second proton transfer to the departing ammonia group via Asp313. The precise role of His246 in this transformation is somewhat ambiguous, but it was postulated that it may be involved in the transfer of a proton from the metal-bound water to Glu217.

In the present study, we use density functional theory (DFT) calculations to elucidate the details of the reaction mechanism of CDA from *Escherichia coli*. A model of the active site is designed on the basis of the crystal structure, and the involved transition states and intermediates are calculated and characterized to present a potential energy profile for the reaction. This approach has been successfully employed to study the reaction mechanisms of a large number of enzymes,[4−8] including many zinc-containing ones.[9−18] It should also be pointed out that the reaction mechanisms of several other deaminases have been studied computationally using various techniques. These include, for example, yeast cytosine deaminase (*y*CD) from *Saccharomyces cerevisiae*,[19−23] cytidine deaminase from *E. coli* (*e*CDA),[24−31] adenosine deaminase (ADA) from *Mus musculus*,[32,33] *t*RNA-specific adenosine deaminase (TadA) from *E. coli*,[34] and guanine deaminase from *Bacillus subtilis* (*b*GD).[35] Some results from these studies will be discussed later when relevant.

II. COMPUTATIONAL DETAILS

All calculations presented in this study were carried out using DFT with the B3LYP functional,[36,37] as implemented in the Gaussian03 software package.[38] Geometry optimizations were performed using the 6-31G(d,p) basis set for the C, N, O, and H elements and the LANL2DZ[39] pseudopotential for Zn. On the basis of these optimized geometries, single-point calculations were conducted with LANL2DZ for Zn and the larger 6-311+G(2d,2p) basis set for the other elements to obtain more accurate energies. Zero-point energy (ZPE) corrections were calculated by performing frequency calculations at the same level of theory as the geometry optimizations. Keeping a number of atoms fixed during the geometry optimizations (see later), leads to several small imaginary frequencies, all below 40*i* cm^{-1} in this case. These frequencies do not contribute significantly to the ZPE and can be ignored. It has in recent years been shown that the addition of empirical dispersion corrections to the B3LYP-calculated energies provides significant improvement of the accuracy.[40−45] In this study, dispersion effects were included according to Grimme's B3LYP-D2 method.[46] The effect of the protein surrounding on the active-site model was estimated by performing single-point calculations using the conductor-like polarizable continuum model (CPCM)[47−50] method at the same level of theory as the geometry optimizations. The dielectric constant was set to the standard value $\varepsilon = 4$ and the UAKS radii were used to specify the cavity. Thus, the final energies reported herein are the large basis set values, corrected for ZPE, solvation, and dispersion effects.

III. RESULTS AND DISCUSSION

III.A. Active-Site Model. A model of the CDA active site was designed on the basis of the crystal structure of the enzyme in complex with the phosphonocytosine inhibitor (PDB entry 3O7U, Figure 1).[2] The model consists of the zinc ion along with its first-shell ligands (His61, His63, and His214), the catalytically important residues Glu217, His246, and Asp313, as well as the residues that make up the pocket where the substrate resides (Leu81, Gln156, and Trp319). The metal-bound inhibitor was manually replaced by a metal-bound water and a cytosine molecule. A water molecule located within hydrogen bonding distance of Glu217 and of the carbonyl oxygen of the inhibitor was also included in the model. This crystallographic water can be seen in the same position in two crystal structures, that is, CDA in complex with phosphonocytosine (PDB entry 3O7U, Figure 1)[2] and 4-(*S*)-hydroxy-3,4-dihydropyrimidine (PDB entry 1K70).[3] The amino acids were truncated either at the α-carbon or at the β-carbon (see Figure 2), and hydrogen atoms were added manually. To maintain the overall structure of the active site and to avoid artificial movements that would be prevented by the protein surrounding, we kept certain atoms at their crystallographic positions during the geometry optimizations, as indicated by

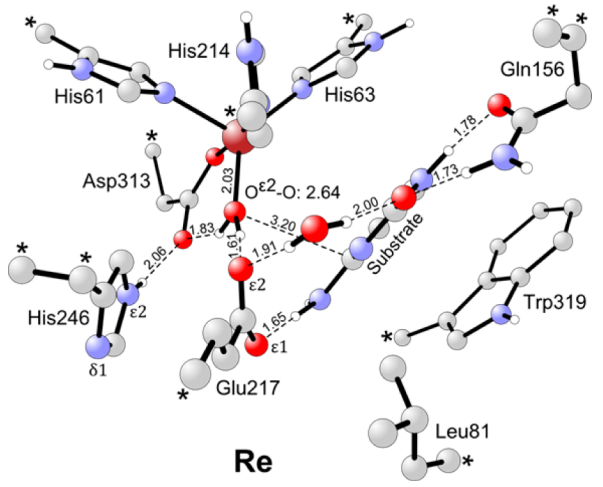

Figure 2. Optimized structure for the CDA active-site model with the cytosine substrate bound (**Re**). Asterisks denote atoms that were kept fixed at their crystallographic positions during the geometry optimization. For clarity, most hydrogen atoms have been omitted in the Figure.

dx.doi.org/10.1021/jp501228s | J. Phys. Chem. B 2014, 118, 5644−5652

Scheme 3. CDA Reaction Mechanism As Suggested by the Present Calculations

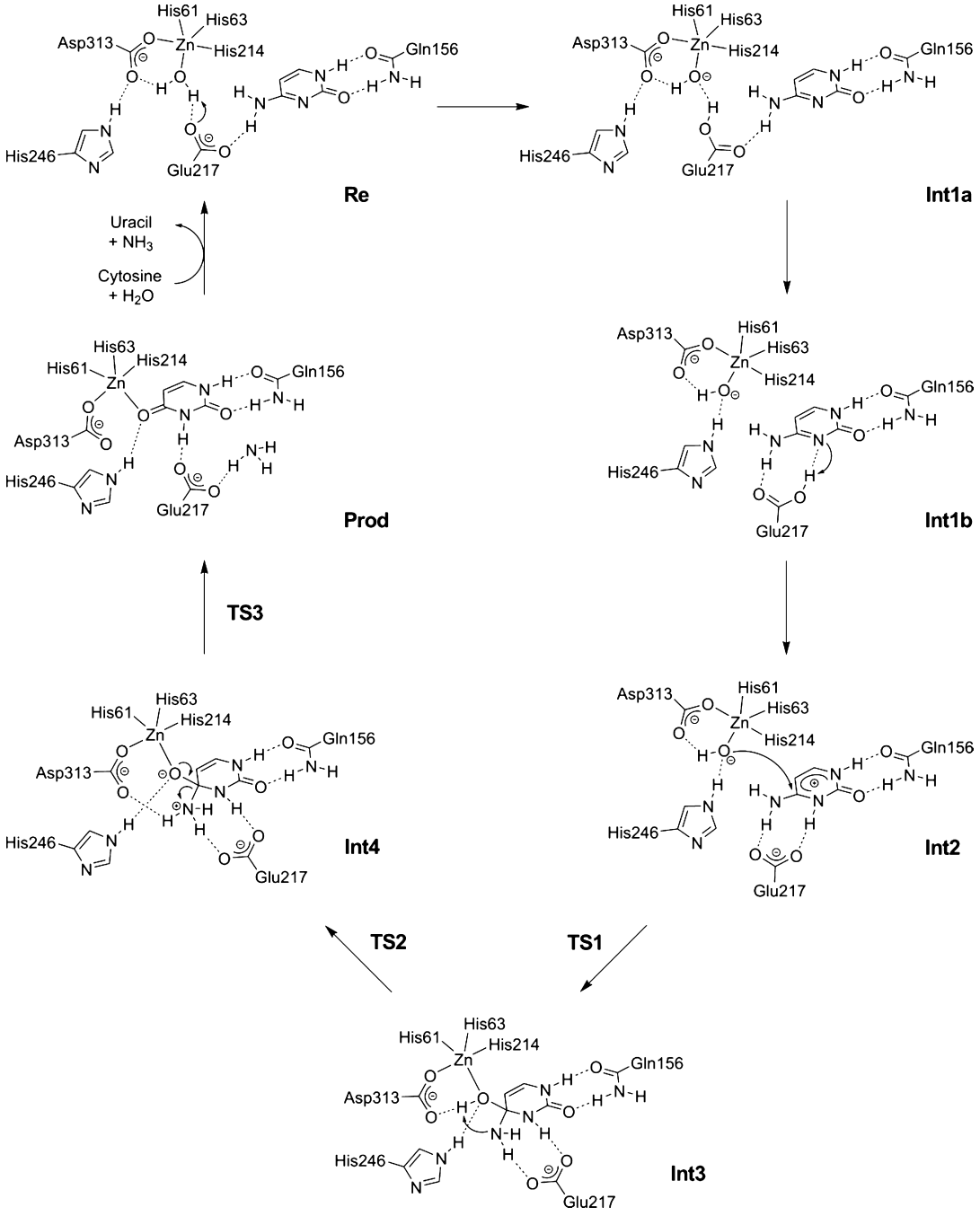

the asterisks in Figure 2. The total size of the active-site model is 145 atoms, and the overall charge is 0.

III.B. Reaction Mechanism. Here we will focus on the mechanism that has the most plausible energies (summarized in Scheme 3). As mentioned in the Introduction, the precise role of His246 is somewhat ambiguous, but it was suggested to function as a proton shuttle, transferring the proton from the metal-bound water nucleophile to Glu217. However, as will be described later, this turned out to be a redundant step because the proton can go directly from the water to the Glu217 residue. The previous suggestion will be discussed at the end of the Results and Discussion section. In the current mechanism, His246 is in the neutral form and the proton is on the $\varepsilon 2$-nitrogen (i.e., the τ tautomer).

The optimized structure of the enzyme−substrate complex (here named **Re** for reactant) is shown in Figure 2. The substrate interacts through several hydrogen bonds with the side chains of Gln156 and Glu217 as well as with the neighboring water molecule present at the active site. These interactions thus position the substrate for the subsequent nucleophilic attack. The metal-bound water forms hydrogen bonds to Asp313 and Glu217, which results in a somewhat different orientation of Glu217 compared with the crystal structure. (See Figures 1 and 2.) In the crystal structure, the side chain of Glu217 is hydrogen bonded to the N(3)H moiety of the inhibitor. However, the substrate does not have a proton on the N3 nitrogen; therefore, as the geometry of the active-site model is optimized in the presence of the substrate, Glu217

dx.doi.org/10.1021/jp501228s | J. Phys. Chem. B 2014, 118, 5644−5652

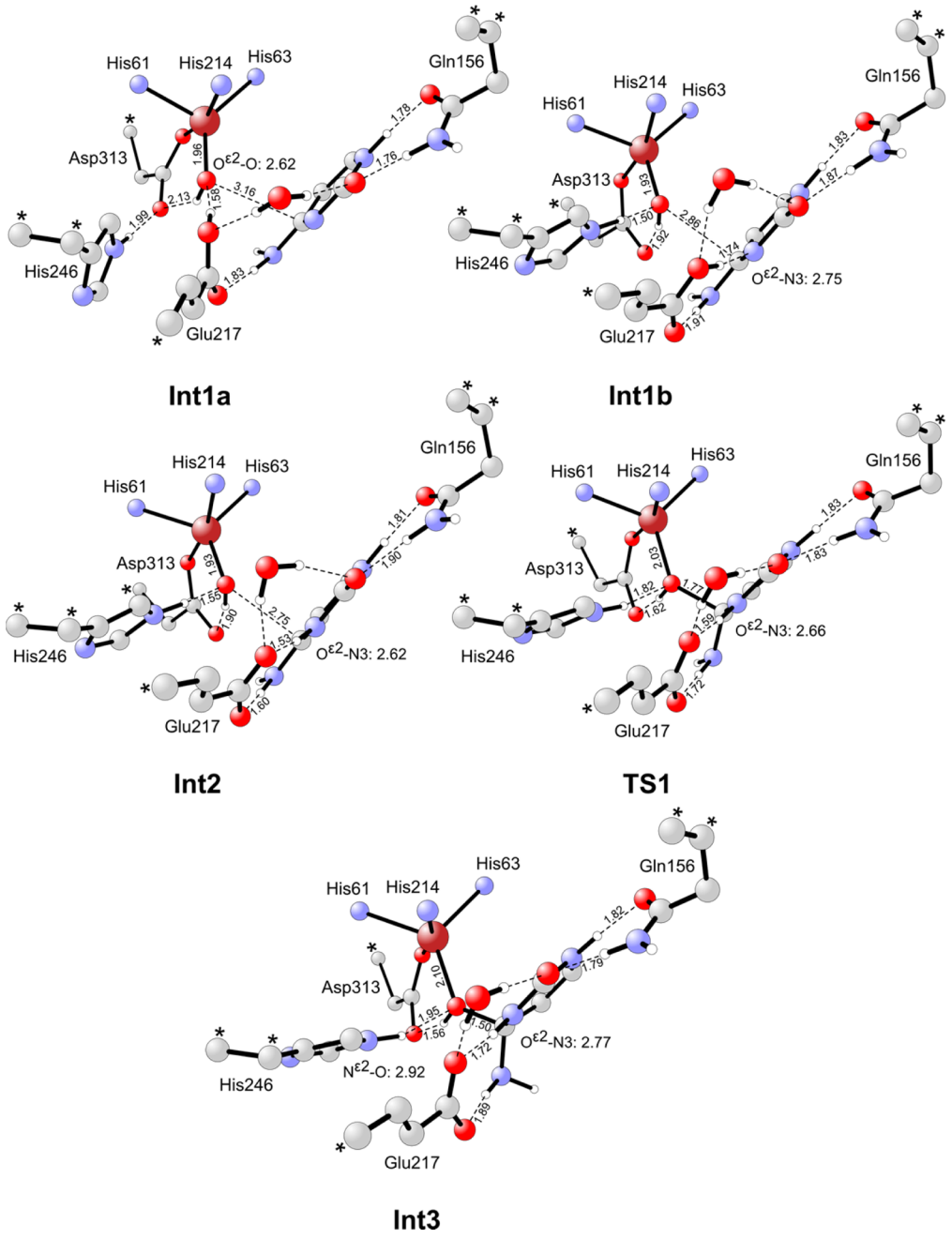

Figure 3. Optimized structures of intermediates and transition states along the reaction pathway. For clarity, Leu81, Trp319, the rings of His61, His63, and His214, and most hydrogen atoms have been omitted. For full model, see Figure 2.

rotates to form a hydrogen bond to the metal-bound water instead. Because the crystal structure in complex with the phosphonocytosine inhibitor is a mimic of the tetrahedral intermediate it should resemble the calculated geometry of that intermediate, which is the case, as will be discussed later. According to this model, the calculations further predict that His246 forms a hydrogen bond to Asp313.

The first step of the reaction is the activation of the metal-bound water nucleophile by a proton transfer to Glu217 (**Re** → **Int1a**, Scheme 3). The optimized structure of intermediate **Int1a** is shown in Figure 3, and the energy is calculated to be 6.1 kcal/mol higher than **Re**. We have optimized the TS for this step, but when all corrections were taken into account (large basis set, ZPE, solvation and dispersion), the energy of the TS was found to be somewhat lower than the energy of **Int1a** (by 2.9 kcal/mol). This is of course an artifact of the adopted methodology (i.e., optimizing in the gas phase with a medium-sized basis set and adding all corrections on the basis of that geometry) and has been previously observed in other examples.[9,15] Therefore, the energy of **Int1a** can effectively be considered as the barrier for this step, and the TS energy is not indicated in the potential energy graph later.

Next, the proton abstracted by Glu217 is to be delivered to the N3 nitrogen of the substrate, but this requires some conformational changes first (**Int1a** → **Int1b**, Scheme 3). Glu217 has to break its hydrogen bond to the nucleophile, rotate toward the substrate, and create a new hydrogen bond to the N3 nitrogen. In addition to this, the calculations indicate that His246 now forms a hydrogen bond to the nucleophile

dx.doi.org/10.1021/jp501228s | J. Phys. Chem. B 2014, 118, 5644−5652

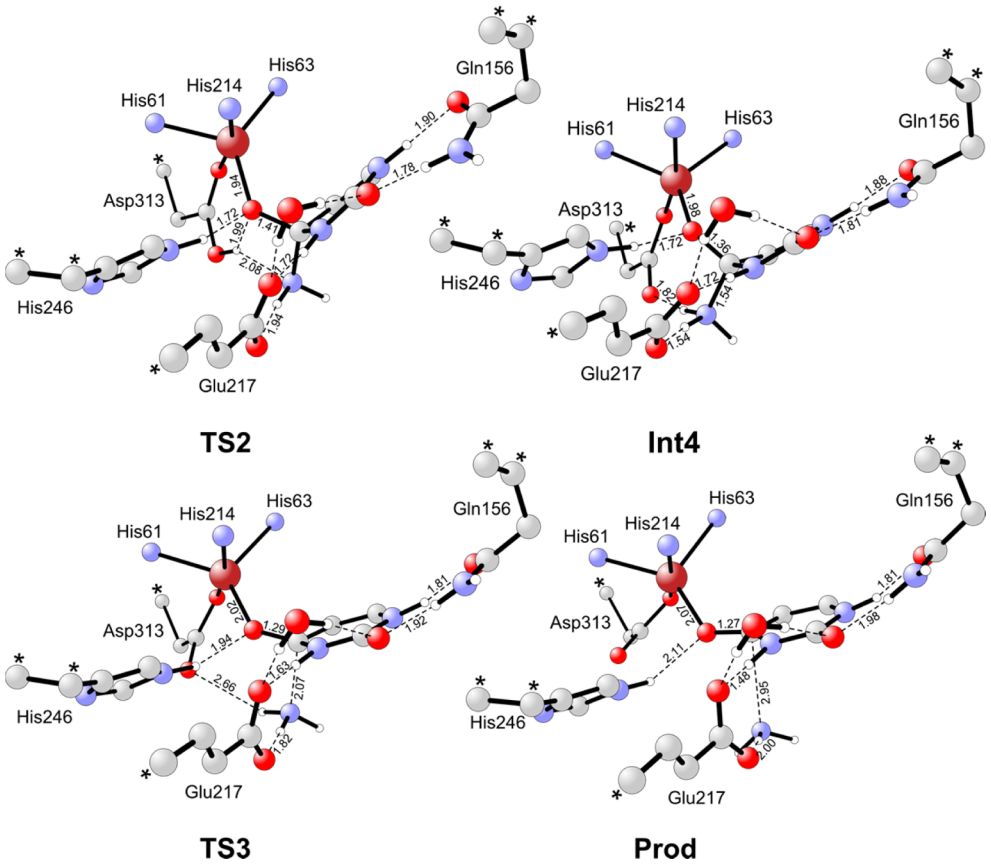

Figure 4. Optimized structures of intermediates and transition states along the reaction pathway. For clarity, Leu81, Trp319, the rings of His61, His63, and His214, and most hydrogen atoms have been omitted. For full model, see Figure 2.

instead of to Asp313. The new intermediate **Int1b** (Figure 3) is 1.5 kcal/mol lower in energy than **Int1a**.

The proton transfer from Glu217 to the N3 nitrogen can now take place, which results in **Int2** (Figure 3) that is 1.4 kcal/mol lower in energy than **Int1b**. We have located the TS also for this proton transfer but similarly to the **Re** → **Int1a** step, after the addition of the corrections the energy becomes slightly lower than for **Int1b** (by 1.2 kcal/mol). Thus, the reaction step can effectively be considered as barrierless.

Hence, according to these calculations, the proton can transfer from the metal-bound water to Glu217 without the need of His246 to function as a shuttle. Performing the initial deprotonation of the metal-bound water nucleophile and the subsequent protonation of the substrate with a single residue could be a common feature of deaminases. For example, the role of Glu217 in CDA is similar to the function of Glu64 in *y*CD,[22,23] Glu104 in *e*CDA,[51] and Glu217 in *Mus musculus* ADA.[32]

The proton on N3 makes the C4 carbon of the substrate more electrophilic and thus more receptive to nucleophilic attack. The optimized structures of the transition state of this nucleophilic attack by the metal-bound hydroxide (**TS1**) and the resulting tetrahedral intermediate (**Int3**) are also shown in Figure 3. Starting at 3.20 Å in **Re**, the critical O−C distance becomes shorter for each intermediate, to reach 1.77 Å at **TS1** and 1.50 Å in **Int3**. The energy barrier for this step is calculated to be 11.0 kcal/mol relative to **Int2,** that is, overall 14.2 kcal/mol relative to **Re**. **Int3** is 3.2 kcal/mol lower in energy than **TS1**.

As previously discussed, the crystal structure in complex with the phosphonocytosine inhibitor is regarded as a mimic of the tetrahedral intermediate.[2] It can thus be compared with the calculated geometry of **Int3**. (See Figures 1 and 3.) We note that there is an overall good resemblance between the two structures, especially in the hydrogen-bonding network of the various residues. For example, in **Int3**, the calculated distance between the *e*2-oxygen of Glu217 and the N3 nitrogen of the tetrahedral intermediate is 2.77 Å, which is in very good agreement with the corresponding crystallographic distance of 2.87 Å. Similarly, the calculated distance between the *e*2-nitrogen of His246 and the hydroxyl oxygen of the tetrahedral intermediate is 2.92 Å, also in very good agreement with the corresponding crystallographic distance of 2.80 Å (i.e., the distance between the *e*2-nitrogen of His246 and the phosphoryl oxygen of the metal-bound inhibitor). This overall agreement provides thus further support to the mechanism suggested by the calculations.

The hydroxyl group has to be deprotonated and the proton delivered to the nitrogen of the leaving group to reach the uracil and ammonia products from **Int3**. It has been suggested that Asp313 assists in this proton transfer.[2] The calculations show that the proton transfer from the hydroxyl to Asp313 and further to the amine group takes place in one concerted step (**TS2**, Figure 4). Despite many attempts, we were not able to locate an intermediate with a protonated Asp313. During the geometry optimization, the proton either goes back to the oxygen or moves to the NH_2 group. The calculated energy of **TS2** is at +13.4 kcal/mol relative to **Re**, which gives a barrier of only 2.4 kcal/mol relative to **Int3**. The critical O−H and H−N

dx.doi.org/10.1021/jp501228s | J. Phys. Chem. B 2014, 118, 5644−5652

distances are 1.99 and 2.08 Å at **TS2**. The geometry of **TS2** is similar to the corresponding TS found in the quantum-chemical study on *Mus musculus* ADA.[32] In ADA, however, the proton transfer is assisted by a histidine residue (corresponding to His246 in CDA) instead of an aspartate.[32] A similar concerted proton-transfer process has been proposed for *E. coli* TadA, although assisted by a glutamate.[34] In contrast, this proton transfer is a stepwise process in *y*CD[22,23] and *b*GD,[35] also assisted by a glutamate.

Downhill from **TS2**, the zwitterionic intermediate **Int4** is calculated to be +3.7 kcal/mol relative to **Re**. Because of the development of negative charge at the hydroxyl oxygen and positive charge at the amine nitrogen the interactions with His246 and Glu217 become stronger, as indicated by the decrease in hydrogen bonding distances (1.95 and 1.89 Å in **Int3**, respectively, and 1.72 and 1.54 Å in **Int4**, respectively; see Figures 3 and 4). Moreover, in **Int4**, there is an additional hydrogen bond between Asp313 and the NH_3 leaving group (1.82 Å), which is not present in the previous intermediate **Int3**. This provides further stabilization to the zwitterionic intermediate.

The next step is the C−N bond cleavage to generate the final uracil and ammonia products (**TS3** and **Prod**, Figure 4). The barrier is calculated to be 8.9 kcal/mol from **Int4**, and the energy of the product complex is 3.5 kcal/mol higher than **Int4**. The scissile C−N bond increases from 1.54 Å in **Int4** to 2.07 Å at **TS3**, while the ammonia is completely detached in **Prod**. As the uracil product is forming, the C−O bond distance decreases from 1.36 Å in **Int4** to 1.27 Å in **Prod**, and the molecular structure becomes more planar.

The products have to be released and the active site regenerated to close the catalytic cycle (**Prod** → **Re**, Scheme 3). With the quantum-chemical methods and models employed in the present study, it is not possible to investigate this process accurately in detail. However, it is possible to estimate the energetics of this step by considering the exothermicity of the overall reaction (Scheme 1), which is calculated to be 3.4 kcal/mol. Because the enzyme does not change this energy, one full catalytic cycle should also be exothermic by 3.4 kcal/mol. This means that the steps involved in the product release and active-site regeneration are together exothermic by 10.6 kcal/mol (i.e., 7.2 + 3.4 kcal/mol, the energy of **Prod** added to the overall exothermicity).

The calculated potential energy profile for the entire reaction is displayed in Figure 5. It indicates that the nucleophilic attack (**TS1**) is the rate-limiting step, with an overall barrier of 14.2 kcal/mol. The experimental rate constant (k_{cat}) has been determined to be 132 s^{-1} for wild-type CDA,[2] which corresponds to a barrier of ca. 15 kcal/mol according to classical transition-state theory. Hence, the calculated barrier is in good agreement with the experimental one. As seen from Figure 5, the energies of **TS1**, **TS2**, and **TS3** are quite close, within 2 kcal/mol, and therefore it cannot based on the energies be excluded that **TS2** or **TS3** might be rate-limiting. However, this would not change the conclusions regarding the reaction mechanism.

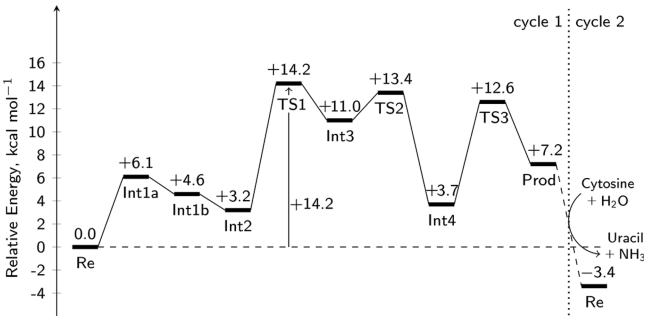

Figure 5. Calculated potential energy profile for the hydrolytic deamination of cytosine by CDA.

The proposed mechanism shown in Scheme 3 is also consistent with the mutagenesis experiments. It has been shown that mutation of either of the residues Gln156, Glu217, His246, or Asp313 results in a significantly decreased catalytic activity,[2] and the calculations can rationalize these findings.

As seen from Figures 2−4, Gln156 is important for the binding of the substrate and its orientation for the nucleophilic attack. Glu217 is essential for the activation of the water nucleophile and the delivering of the proton to the substrate. Asp313, in turn, is essential for the deprotonation of the tetrahedral intermediate and the protonation of the leaving group. Finally, the role of His246 is somewhat less straightforward to rationalize. In the initial part of the mechanism (**Re** and **Int1a**), His246 forms a hydrogen bond to the Asp313 residue to then shift to form a hydrogen bond to the nucleophile. This interaction might stabilize the intermediates and transition states, thereby lowering the barriers, especially in the steps (**Int3** → **TS2** → **Int4**). Very importantly, when this hydrogen bond is not there, that is, in a model where the proton of the histidine is located at the δ1-nitrogen, the barrier for the nucleophilic attack is calculated to be higher in energy. (See the SI for details.)

Here it is interesting to compare the calculated reaction mechanism of CDA with the mechanisms of some other deaminases. The suggested reaction path of CDA resembles mainly those proposed for *Mus musculus* ADA[32] and *b*GD,[35] in the sense that two different residues are involved in the proton transfer events. The roles of Glu217 and Asp313 in CDA are performed by Asp114 and Glu55 in *b*GD[35] and Glu217 and His238 in ADA.[32] In *y*CD and *e*CDA, only one residue functions as a proton shuttle throughout the reaction, Glu64 in *y*CD[22,23] and Glu104 in *e*CDA.[51] Although both CDA and *y*CD catalyze the deamination of cytosine, the active-site architectures are significantly different between the two enzymes,[52] which explains the differences in reaction mechanisms. The *y*CD-active site is rather similar to that of *e*CDA, in that the zinc ion has one histidine and two cysteines as first-shell ligands and there is a glutamate base.[53] *b*GD also shares these active-site features, although it has an additional aspartate,[54] that according to ONIOM calculations is the residue that performs the initial proton transfer.[35]

III.C. Kinetic Isotope Effect. Kinetic studies with D_2O as a solvent showed that CDA exhibits an inverse deuterium isotope effect of 0.62 ± 0.01 on k_{cat};[2] that is, the hydrolytic deamination of cytosine is faster in D_2O than in H_2O. This effect was ascribed to the formation of a low-barrier hydrogen bond between Glu217 and the N3 nitrogen of the substrate prior to the nucleophilic attack.[2]

As seen from Figure 3, the distance between the ε2-oxygen of Glu217 and the N3 nitrogen in **Int2** is 2.62 Å, only slightly longer than the expected distance for a low-barrier hydrogen bond, which is ∼2.55 Å.[55] At the nucleophilic attack transition state **TS1** this distance is increased to 2.66 Å, and at the tetrahedral intermediate **Int3** it is 2.77 Å, which is the distance of a normal hydrogen bond.

dx.doi.org/10.1021/jp501228s | J. Phys. Chem. B 2014, 118, 5644−5652

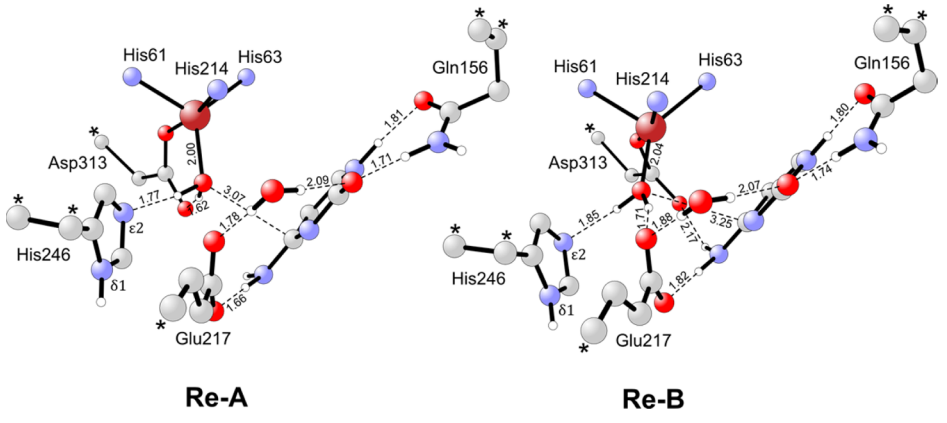

Figure 6. Optimized structures for the CDA active-site model in the case of Nδ1-protonted His246. For clarity, Leu81, Trp319, the rings of His61, His63, and His214, and most hydrogen atoms have been omitted. For full model, see Figure 2.

To examine whether the calculations can reproduce the experimental results, we have estimated the KIE by recalculating the ZPEs using the mass of deuterium instead of proton for the two water molecules in **Int2** and the rate-limiting **TS1**. Using classical transition-state theory, the computed ZPE differences can be converted into a ratio of rate constants and thus a kinetic isotope effect. The calculations yield indeed a barrier decrease of 0.17 kcal/mol, which corresponds to an inverse isotope effect of 0.74, in good agreement with the experimental value.

However, according to the calculated potential energy profile (Figure 5), **Re** is the resting state of the catalytic cycle (3.2 kcal/mol lower than **Int2**), and the KIE should therefore be evaluated from the ZPE differences between **TS1** and **Re**. In this case, the calculated barrier decrease is 0.08 kcal/mol, corresponding to an inverse KIE of 0.86, which is also in line with the experimental results. Recalculating the isotope effect by exchanging one proton at a time confirms that almost all of the effect originates from the proton of the metal-bound water that is hydrogen bonded to Glu217 and later transferred to the substrate. The O−O hydrogen bonding distance in **Re** is also quite short, 2.64 Å (see Figure 2), which explains the observed inverse isotope effect.

The above KIE calculations provide thus further corroboration for the suggested mechanism of Scheme 3. Here it should be pointed out that the calculated energy difference between **Int2** and **Re** is rather small, only 3.2 kcal/mol, and could fall within the error margin of the employed methodology. Therefore, it cannot be excluded that **Int2** could be the resting state of the cycle, in which case the calculated KIE would also be consistent with the experiments, as previously shown.

III.D. On the Alternative Role of His246. The mechanism proposed by the calculations (Scheme 3) assumes that the proton of the neutral His246 is on the ε2-nitrogen (τ tautomer). However, as previously discussed, His246 has previously been ascribed a role as a proton shuttle, transferring the proton from the metal-bound water to Glu217.[2] This scenario requires the proton to be on the δ1-nitrogen (π tautomer). The suggestion was based on the fact that Glu217 in the X-ray structures of CDA, in both the absence and presence of inhibitors (PDB entries 1K6W, 1K70, and 3O7U), appears to be too far away from the metal-bound water for the direct abstraction of the proton.[2] Another indication is the fact that the E217A mutant is able to catalyze the hydrolysis of the substrate analogue 3-oxauracil, which does not require protonation of the O3 oxygen (that corresponds to the N3 nitrogen).[2]

However, the crystal structure in complex with the phosphonocytosine inhibitor shows that His246 is in close distance from Asn279 (Figure 1) and can thus accept a hydrogen bond from it, which indicates that the proton should be at the ε2-nitrogen. Also, as seen from the optimized structure of the active-site model (Figure 2), there is a direct hydrogen bond between the zinc-bound water and Glu217 when the inhibitor is replaced by the cytosine substrate and a metal-bound water molecule. Direct transfer of the proton from the water to Glu217 was furthermore previously shown to be associated with a very low energy cost (Figure 5). In addition, it should also be remembered that the crystal structure in complex with phosphonocytosine is a mimic of the tetrahedral intermediate. As previously shown, the calculated geometry of **Int3** resembles quite well the crystal structure. In this intermediate, Glu217 has rotated away from the metal-bound water and delivered the proton to the substrate, thereof the large distance between it and the water nucleophile.

All of these facts speak in favor of His246 being protonated at the ε2-nitrogen. Nevertheless, we have in this study explicitly considered the scenario in which the proton of His246 is on the δ1-nitrogen. In this case, two different structures of the ES complex were located in which the nucleophilic water forms a hydrogen bond to His246. The optimized structures (called **Re-A** and **Re-B**) are shown in Figure 6. In the two structures the substrate interacts with Gln156, Glu217, and the neighboring water, such that it is properly oriented and ready for the subsequent nucleophilic attack, analogously to the case in **Re** (Figure 2). However, in **Re-A**, the hydrogen bond to Glu217 is replaced by a hydrogen bond to His246 instead, while in **Re-B** the metal-bound water is hydrogen bonded to His246 and Glu217, and Asp313 is interacting with the NH_2 group of the substrate.

It turns out that the calculated energies of these structures are higher than those of **Re**, by 10.4 and 6.5 kcal/mol, for **Re-A** and **Re-B**, respectively. However, it should be pointed out that these energies could change somewhat if a larger active-site model is employed, especially in the region around the histidine. Apart from being higher in energy compared with **Re**, starting from either **Re-A** or **Re-B**, the calculations show that His246 is not able to abstract the proton, which is the first step in the suggested proton shuttle pathway. All attempts to

dx.doi.org/10.1021/jp501228s | J. Phys. Chem. B 2014, 118, 5644−5652

locate the intermediate with protonated His246 resulted in the proton going back to the hydroxide and reforming the water during the optimization. Moreover, performing the nucleophilic attack directly from **Re-A** or **Re-B** resulted in the breaking of the water-histidine hydrogen bond and the formation of a hydrogen bond to either Glu217 in the case of **Re-A** or Asp313 in the case of **Re-B**. That is, both these structures lead to transition states for the nucleophilic attack that are very similar to the one found starting from **Re** (**TS1**). Overall, these calculations thus indicate that the histidine is unlikely to function as a proton shuttle in the deamination reaction.

Finally, it should be noted that we also found another structure with the His246 protonated at the Nδ1 position but in which there is no hydrogen bond between the nucleophilic water and the histidine. In this case, the reaction followed the same mechanism as in Scheme 3, but the calculated barrier for the nucleophilic attack was ca. 5 kcal/mol higher than for **TS1**. (See the SI for details.)

IV. CONCLUSIONS

We have investigated the reaction mechanism of the zinc-dependent cytosine deaminase from *Escherichia coli* using DFT calculations. The obtained reaction mechanism is summarized in Scheme 3, and the associated potential energy profile is presented in Figure 5. Our calculations support the main features of the previously proposed mechanism, the main difference being the role of the His246 residue. In the current mechanism, His246 is in the neutral form, and the proton is on the ε2-nitrogen (i.e., the τ tautomer). The following mechanistic features can be established from the calculations. The initial deprotonation of the metal-bound water nucleophile was found to be affected by Glu217 without the need of a proton shuttle to transfer the proton from the metal-bound water to Glu217. His246 has previously been ascribed this role. However, our calculations demonstrate that His246 is unlikely to function as a proton shuttle. Protonation of the ring nitrogen of the cytosine substrate by Glu217 was found to occur prior to the nucleophilic attack by the metal-bound hydroxide, while deprotonation of the tetrahedral intermediate and protonation of the leaving group was found to take place in one concerted step assisted by Asp313. The calculations indicate that the nucleophilic attack is the rate-limiting step with an overall barrier in good agreement with the experimental value. Finally, the experimentally determined inverse solvent deuterium isotope effect was reproduced by the calculations, which provides further support to the suggested mechanism.

■ ASSOCIATED CONTENT

Supporting Information

Full reference for Gaussian, additional results concerning the other protonation state of His246, and Cartesian coordinates of all stationary points. This material is available free of charge via the Internet at http://pubs.acs.org.

■ AUTHOR INFORMATION

Corresponding Author

*E-mail: himo@organ.su.se. Tel: +46 8 161094.

Notes

The authors declare no competing financial interest.

■ ACKNOWLEDGMENTS

F.H. acknowledges financial support from the Swedish Research Council, the Göran Gustafsson Foundation, and the Knut and Alice Wallenberg Foundation. Computer time was generously provided by the Swedish National Infrastructure for Computing. F.M.R. acknowledges support from the Robert A. Welch Foundation (A-840). We also thank Dr. Rong-Zhen Liao for valuable discussions.

■ REFERENCES

(1) Seibert, C. M.; Raushel, F. M. Structural and Catalytic Diversity within the Amidohydrolase Superfamily. *Biochemistry* **2005**, *44*, 6383−6391.
(2) Hall, R. S.; Fedorov, A. A.; Xu, C.; Fedorov, E. V.; Almo, S. C.; Raushel, F. M. Three-Dimensional Structure and Catalytic Mechanism of Cytosine Deaminase. *Biochemistry* **2011**, *50*, 5077−5085.
(3) Ireton, G. C.; McDermott, G.; Black, M. E.; Stoddard, B. L. The Structure of Escherichia Coli Cytosine Deaminase. *J. Mol. Biol.* **2002**, *315*, 687−697.
(4) Siegbahn, P. E. M.; Himo, F. The Quantum Chemical Cluster Approach for Modeling Enzyme Reactions. *Wiley Interdiscip. Rev.: Comput. Mol. Sci.* **2011**, *1*, 323−336.
(5) Blomberg, M. R. A; Siegbahn, P. E. M. Quantum Chemistry as a Tool in Bioenergetics. *Biochim. Biophys. Acta* **2010**, *1797*, 129−142.
(6) Siegbahn, P. E. M.; Himo, F. Recent Developments of the Quantum Chemical Cluster Approach for Modeling Enzyme Reactions. *J. Biol. Inorg. Chem.* **2009**, *14*, 643−651.
(7) Siegbahn, P. E. M.; Borowski, T. Modeling Enzymatic Reactions Involving Transition Metals. *Acc. Chem. Res.* **2006**, *39*, 729−738.
(8) Himo, F. Quantum Chemical Modeling of Enzyme Active Sites and Reaction Mechanisms. *Theor. Chem. Acc.* **2006**, *116*, 232−240.
(9) Chen, S.-L.; Li, Z.-S.; Fang, W.-H. Theoretical Investigation of Astacin Proteolysis. *J. Inorg. Biochem.* **2012**, *111*, 70−79.
(10) Amata, O.; Marino, T.; Russo, N.; Toscano, M. A Proposal for Mitochondrial Processing Peptidase Catalytic Mechanism. *J. Am. Chem. Soc.* **2011**, *133*, 17824−17831.
(11) Alberto, M. E.; Leopoldini, M.; Russo, N. Can Human Prolidase Enzyme Use Different Metals for Full Catalytic Activity. *Inorg. Chem.* **2011**, *50*, 3394−3403.
(12) Amata, O.; Marino, T.; Russo, N.; Toscano, M. Catalytic Activity of a ζ-Class Zinc and Cadmium Containing Carbonic Anhydrase. Compared work mechanisms. *Phys. Chem. Chem. Phys.* **2011**, *13*, 3468−3477.
(13) Liao, R.-Z.; Yu, J.-G.; Himo, F. Phosphate Mono- and Diesterase Activities of the Trinuclear Zinc Enzyme Nuclease P1 − Insights from Quantum Chemical Calculations. *Inorg. Chem.* **2010**, *49*, 6883−6888.
(14) Liao, R.-Z.; Yu, J.-G.; Himo, F. Reaction Mechanism of the Trinuclear Zinc Enzyme Phospholipase C: A Density Functional Theory Study. *J. Phys. Chem. B* **2010**, *114*, 2533−2540.
(15) Liao, R.-Z.; Himo, F.; Yu, J.-G.; Liu, R.-Z. Dipeptide Hydrolysis by the Dinuclear Zinc Enzyme Human Renal Dipeptidase: Mechanistic Insights from DFT calculations. *J. Inorg. Biochem.* **2010**, *104*, 37−46.
(16) Amata, O.; Marino, T.; Russo, N.; Toscano, M. Human Insulin-Degrading Enzyme Working Mechanism. *J. Am. Chem. Soc.* **2009**, *131*, 14804−14811.
(17) Liao, R.-Z.; Himo, F.; Yu, J.-G.; Liu, R.-Z. Theoretical Study of the RNA Hydrolysis Mechanism of the Dinuclear Zinc Enzyme RNase Z. *Eur. J. Inorg. Chem.* **2009**, *20*, 2967−2972.
(18) Liao, R.-Z.; Yu, J.-G.; Himo, F. Reaction Mechanism of the Dinuclear Zinc Enzyme N-Acyl-L-Homoserine Lactone Hydrolase: A Quantum Chemical Study. *Inorg. Chem.* **2009**, *48*, 1442−1448.
(19) Matsubara, T.; Dupuis, M.; Aida, M. An Insight into the Environmental Effects of the Pocket of the Active Site of the Enzyme. Ab Initio ONIOM-Molecular Dynamics (MD) Study on Cytosine Deaminase. *J. Comput. Chem.* **2008**, *29*, 458−465.

(20) Yao, L.; Yan, H.; Cukier, R. I. A Molecular Dynamics Study of the Ligand Release Path in Yeast Cytosine Deaminase. *Biophys. J.* **2007**, *92*, 2301−2310.
(21) Yao, L.; Yan, H.; Cukier, R. I. A Combined ONIOM Quantum Chemical-Molecular Dynamics Study of Zinc-Uracil Bond Breaking in Yeast Cytosine Deaminase. *J. Phys. Chem. B* **2006**, *110*, 26320−26326.
(22) Yao, L.; Sklenak, S.; Yan, H.; Cukier, R. I. A Molecular Dynamics Exploration of the Catalytic Mechanism of Yeast Cytosine Deaminase. *J. Phys. Chem. B* **2005**, *109*, 7500−7510.
(23) Sklenak, S.; Yao, L.; Cukier, R. I.; Yan, H. Catalytic Mechanism of Yeast Cytosine Deaminase: An ONIOM Computational Study. *J. Am. Chem. Soc.* **2004**, *126*, 14879−14889.
(24) Matsubara, T.; Dupuis, M.; Aida, M. Ab Initio ONIOM-Molecular Dynamics (MD) Study on the Deamination Reaction by Cytidine Deaminase. *J. Phys. Chem. B* **2007**, *111*, 9965−9974.
(25) Matsubara, T.; Dupuis, M.; Aida, M. The ONIOM Molecular Dynamics Method for Biochemical Applications: Cytidine Deaminase. *Chem. Phys. Lett.* **2007**, *437*, 138−142.
(26) Matsubara, T.; Ishikura, M.; Aida, M. A Quantum Chemical Study of the Catalysis for Cytidine Deaminase: Contribution of the Extra Water Molecule. *J. Chem. Inf. Model.* **2006**, *46*, 1276−1285.
(27) Guo, H.; Rao, N.; Xu, Q.; Guo, H. Origin of Tight Binding of a Near-Perfect Transition-State Analogue by Cytidine Deaminase: Implications for Enzyme Catalysis. *J. Am. Chem. Soc.* **2005**, *127*, 3191−3197.
(28) Xu, Q.; Guo, H. Quantum Mechanical/Molecular Mechanical Molecular Dynamics Simulations of Cytidine Deaminase: From Stabilization of Transition State Analogues to Catalytic Mechanisms. *J. Phys. Chem. B* **2004**, *108*, 2477−2483.
(29) Kedzierski, P.; Sokalski, W. A.; Cheng, H.; Mitchell, J.; Leszczynski, J. DFT Study of the Reaction Proceeding in the Cytidine Deaminase. *Chem. Phys. Lett.* **2003**, *381*, 660−665.
(30) Lewis, J. P.; Liu, S.; Lee, T.-S.; Yang, W. A Linear-Scaling Quantum Mechanical Investigation of Cytidine Deaminase. *J. Comput. Phys.* **1999**, *151*, 242−263.
(31) Lewis, J. P.; Carter, C. W., Jr.; Hermans, J.; Pan, W.; Lee, T.-S.; Yang, W. Active Species for the Ground-State Complex of Cytidine Deaminase: A Linear-Scaling Quantum Mechanical Investigation. *J. Am. Chem. Soc.* **1998**, *120*, 5407−5410.
(32) Wu, X.-H.; Zou, G.-L.; Quan, J.-M.; Wu, Y.-D. A Theoretical Study on the Catalytic Mechanism of Mus Musculus Adenosine Deaminase. *J. Comput. Chem.* **2010**, *31*, 2238−2247.
(33) Gleeson, M. P.; Burton, N. A.; Hillier, I. H. The Mechanism of Adenosine Deaminase Catalysis Studied by QM/MM Calculations: The Role of Histidine 238 and the Activity of the Alanine 238 Mutant. *Phys. Chem. Chem. Phys.* **2003**, *5*, 4272−4278.
(34) Luo, M.; Schramm, V. L. Transition State Structure of E. Coli tRNA-Specific Adenosine Deaminase. *J. Am. Chem. Soc.* **2008**, *130*, 2649−2655.
(35) Yao, L.; Cukier, R. I.; Yan, H. Catalytic Mechanism of Guanine Deaminase: An ONIOM and Molecular Dynamics Study. *J. Phys. Chem. B* **2007**, *111*, 4200−4210.
(36) Becke, A. D. Density-Functional Thermochemistry. III. The Role of Exact Exchange. *J. Chem. Phys.* **1993**, *98*, 5648−5652.
(37) Lee, C.; Yang, W.; Parr, R. G. Development of the Colle-Salvetti Correlation-Energy Formula into a Functional of the Electron Density. *Phys. Rev. B* **1988**, *37*, 785−789.
(38) Frisch, M. J.; Trucks, G. W.; Schlegel, H. B.; Scuseria, G. E.; Robb, M. A.; Cheeseman, J. R.; Montgomery, J. A. Jr.; Vreven, T.; Kudin, K. N.; Burant, J. C., et al. *Gaussian 03*, revision D.01 and E.01; Gaussian, Inc.: Wallingford, CT, 2004.
(39) Hay, P. J.; Wadt, W. R. Ab Initio Effective Core Potentials for Molecular Calculations. Potentials for the Transition Metal Atoms Sc to Hg. *J. Chem. Phys.* **1985**, *82*, 270−283.
(40) Minenkov, Y.; Occhipinti, G.; Jensen, V. R. Metal−Phosphine Bond Strengths of the Transition Metals: A Challenge for DFT. *J. Phys. Chem. A* **2009**, *113*, 11833−11844.
(41) Siegbahn, P. E. M.; Blomberg, M. R. A.; Chen, S.-L. Significant van der Waals Effects in Transition Metal Complexes. *J. Chem. Theory Comput.* **2010**, *6*, 2040−2044.
(42) Lonsdale, R.; Harvey, J. N.; Mulholland, A. J. Inclusion of Dispersion Effects Significantly Improves Accuracy of Calculated Reaction Barriers for Cytochrome P450 Catalyzed Reactions. *J. Phys. Chem. Lett.* **2010**, *1*, 3232−3237.
(43) Osuna, S.; Swart, M.; Solà, M. Dispersion Corrections Essential for the Study of Chemical Reactivity in Fullerenes. *J. Phys. Chem. A* **2011**, *115*, 3491−3496.
(44) Santoro, S.; Liao, R.-Z.; Himo, F. Theoretical Study of Mechanism and Selectivity of Copper-Catalyzed C−H Bond Amidation of Indoles. *J. Org. Chem.* **2011**, *76*, 9246−9252.
(45) Xu, X.; Liu, P.; Lesser, A.; Sirois, L. E.; Wender, P. A.; Houk, K. N. Ligand Effects on Rates and Regioselectivities of Rh(I)-Catalyzed (5 + 2) Cycloadditions: A Computational Study of Cyclooctadiene and Dinaphthocyclooctatetraene as Ligands. *J. Am. Chem. Soc.* **2012**, *134*, 11012−11025.
(46) Grimme, S. Semiempirical GGA-Type Density Functional Constructed with a Long-Range Dispersion Correction. *J. Comput. Chem.* **2006**, *27*, 1787−1799.
(47) Klamt, A.; Schüürmann, G. COSMO: A New Approach to Dielectric Screening in Solvents with Explicit Expressions for the Screening Energy and its Gradient. *J. Chem. Soc., Perkin Trans.* **1993**, *2*, 799−805.
(48) Andzelm, J.; Kölmel, C.; Klamt, A. Incorporation of Solvent Effects into Density Functional Calculations of Molecular Energies and Geometries. *J. Chem. Phys.* **1995**, *103*, 9312−9320.
(49) Barone, V.; Cossi, M. Quantum Calculation of Molecular Energies and Energy Gradients in Solution by a Conductor Solvent Model. *J. Phys. Chem. A* **1998**, *102*, 1995−2001.
(50) Cossi, M.; Rega, N.; Scalmani, G.; Barone, V. Energies, Structures, and Electronic Properties of Molecules in Solution with the C-PCM Solvation Model. *J. Comput. Chem.* **2003**, *24*, 669−681.
(51) Snider, M. J.; Reinhardt, L.; Wolfenden, R.; Cleland, W. W. ^{15}N Kinetic Isotope Effects on Uncatalyzed and Enzymatic Deamination of Cytidine. *Biochemistry* **2002**, *41*, 415−421.
(52) Ireton, G. C.; Black, M. E.; Stoddard, B. L. The 1.14 Å Crystal Structure of Yeast Cytosine Deaminase: Evolution of Nucleotide Salvage Enzymes and Implications for Genetic Chemotherapy. *Structure* **2003**, *11*, 961−972.
(53) Ko, T.-P.; Lin, J.-J.; Hu, C.-Y.; Hsu, Y.-H.; Wang, A. H.-J.; Liaw, S.-H. Crystal Structure of Yeast Cytosine Deaminase: Insights into Enzyme Mechanism and Evolution. *J. Biol. Chem.* **2003**, *278*, 19111−19117.
(54) Liaw, S.-H.; Chang, Y.-J.; Lai, C.-T.; Chang, H.-C.; Chang, G.-G. Crystal Structure of Bacillus Subtilis Guanine Deaminase: The First Domain-Swapped Structure in the Cytidine Deaminase Superfamily. *J. Biol. Chem.* **2004**, *279*, 35479−35485.
(55) Cleland, W. W.; Frey, P. A.; Gerlt, J. A. The Low Barrier Hydrogen Bond in Enzymatic Catalysis. *J. Biol. Chem.* **1998**, *273*, 25529−25532.